



Auger electron spectroscopy analysis of high metal content micro-structures grown by electron beam induced deposition

F. Cicoira^{a,1}, P. Hoffmann^{a,*}, C.O.A. Olsson^b, N. Xanthopoulos^b,
H.J. Mathieu^b, P. Doppelt^c

^aLaboratoire d'Optique Appliquée (LOA), Ecole Polytechnique Fédérale de Lausanne, CH-1015 Lausanne EPFL, Switzerland

^bLaboratoire de Métallurgie Chimique (LMCH), Ecole Polytechnique Fédérale de Lausanne,
CH-1015 Lausanne EPFL, Switzerland

^cCentre d'Etude de Chimie Métallurgique (CNRS), 15 rue Georges Urbain, 94407 Vitry sur Seine, France

Received in revised form 3 August 2004; accepted 3 August 2004

Available online 27 September 2004

Abstract

An auger electron spectroscopy study was carried out on Rh-containing micro-structures grown by electron beam induced deposition (EBID) of the iso-structural and iso-electronic precursors $[\text{RhCl}(\text{PF}_3)_2]_2$ and $[\text{RhCl}(\text{CO})_2]_2$. A material containing between 55 and 60 at.% Rh was obtained from both precursors. The chemical composition of structures grown from the two different precursors indicates a similar decomposition mechanism. Deposits grown from $[\text{RhCl}(\text{PF}_3)_2]_2$ showed a chemical composition independent of electron energy and electron dose in the investigated range of conditions.

© 2004 Elsevier B.V. All rights reserved.

PACS: 82.80.Pv; 81.15.Jj; 81.70.Jb; 85.40.Ux

Keywords: Chemical vapor deposition; Auger electron spectroscopy; Nanomaterials

1. Introduction

Electron beam induced deposition (EBID) is a very attractive nano-fabrication technique, which has already allowed small-scale production of nano-devices [1–9]. One of the limitations of EBID is the lack of control of the chemical composition of the deposited material, due to the non-equilibrium character of the decomposition process. Attempts to

* Corresponding author. Tel.: +41 21 6936018;
fax: +41 21 6933701.

E-mail address: f.cicoira@ism.bo.cnr.it (F. Cicoira),
patrik.hoffmann@epfl.ch (P. Hoffmann).

¹ Present address: Istituto per lo Studio dei Materiali Nanos-trutturati (ISMN), CNR, via Gobetti 101, 40129 Bologna, Italy.

Table 1

Properties and data of the rhodium precursors used in this work: molecular formula, molecular weight (M), vapor pressure (P_{vap}) at ambient temperature, Rh atomic percent (Rh at.%), Rh oxidation number (n_{ox}), chemical abstract system (CAS) number

Formula	M (g mol ⁻¹)	P_{vap} (Pa) at 21 °C	Rh at. %	n_{ox}	CAS number
Cl ₂ F ₁₂ P ₄ Rh ₂	628.59	7.47 [15]	10	+1	14876-98-3
C ₄ Cl ₂ O ₄ Rh ₂	388.76	0.25 [19]	20	+1	14404-25-2

produce metallic deposits resulted, with few exceptions [7,10], in nano-composite materials with variable metal content, made up of metallic nanocrystals embedded in an amorphous matrix of precursor ligand elements.

The precursor di- η -chloro tetrakis (phosphorous trifluoride)-di-rhodium, [RhCl(PF₃)₂]₂ (CAS 14876-98-3) is very interesting for the EBID of metals, since it is carbon-free, volatile and easy to synthesize. [RhCl(PF₃)₂]₂ has been already used as a precursor in thermal chemical vapor deposition (CVD) [11], scanning tunneling microscopy (STM) direct writing [12], and EBID [6,13,14]. This compound has been widely studied over the last few years: vapor pressure [15] and mass spectrometry data together with theoretical calculations of the possible decomposition paths [16] are available. Morphological, structural and chemical analysis performed by transmission electron microscopy (TEM) and electron energy loss spectroscopy (EELS) has shown that the deposited material is a nanocomposite, containing the elements Rh, P, Cl, O and N [17].

In this work we present an auger electron spectroscopy (AES) study of micro-structures grown by EBID of [RhCl(PF₃)₂]₂ and, for a comparative study, of the iso-structural and iso-electronic precursor [RhCl(CO)₂]₂, tetracarbonyl di- η -chloro di-rhodium (CAS 14404-25-2). AES is of interest for analysis of structures grown by EBID since it allows analysis on bulk samples, combining high elemental sensitivity, high lateral and in depth resolution with high resolution imaging in the analysis chamber. The electron ionization mass spectra of both [RhCl(PF₃)₂]₂ [13] and [RhCl(CO)₂]₂ [18] show a similar decomposition path, consisting of progressive loss of non-bridging groups bonded to the Rh atoms (namely CO and PF₃). [RhCl(CO)₂]₂ is, in principle, less attractive than [RhCl(PF₃)₂]₂ for EBID since it is less volatile [19] and not carbon-free. Nevertheless a comparison of the chemical composition of EBID structures grown

from the two precursors can be helpful for a better understanding of the decomposition mechanism.

2. Experimental

The EBID deposition apparatus used in this work is based on a modified scanning electron microscope (SEM) Cambridge S100 fitted with a tungsten filament thermionic electron gun. A more detailed description of the apparatus can be found elsewhere [6,7,13,14,17]. [RhCl(PF₃)₂]₂ was synthesized following a known procedure [20], whereas [RhCl(CO)₂]₂ is commercially available (Fluka, 36065). Some data and properties of [RhCl(PF₃)₂]₂ and [RhCl(CO)₂]₂ are listed in Table 1. The EBID rate is mainly determined by the vapor pressure of the precursor [21]. Therefore the vapor pressures of the precursors used in this work are reported in column 3 of Table 1. The values refer to the applied experimental conditions, i.e. ambient temperature (21 °C).

The deposits were grown on naturally oxidized p-doped Si(1 1 1) in the form of squares, with sides ranging from 5 to 20 μm and thickness ranging from 1 to 5 μm . During deposition the electron beam was operated in scanning mode, along a TV frame in a standard scan of 625 lines with a frequency of 3.75 Hz. Several samples were grown using various electron energies (E), electron probe currents (I_p) and exposure times (t_e). The deposition parameters of samples whose spectra are shown below are listed in Table 2.

Table 2
Deposition parameters of the structures whose spectra are shown in this work

No.	Precursor	Energy (eV)	Current (nA)
1	[RhCl(PF ₃) ₂] ₂	25	2.2
2	(CH ₃)Au(tfa)	25	2
3	[RhCl(PF ₃) ₂] ₂	5	10
4	[RhCl(CO) ₂] ₂	25	2.2

The Rh standard used for AES was a pure Rh foil (purity 99.8%, Alfa Aesar). As a reference for the C peak, we used a high C content deposit grown by EBID of the precursor dimethyl-gold trifluoro-acetyl acetate, $(\text{CH}_3)_2\text{Au}(\text{tfa})$ (chemical formula $\text{C}_7\text{H}_{10}\text{O}_2\text{F}_3\text{Au}$, CAS 63470-53-1).

AES analysis was performed ex situ with a PHI 660 (Perkin-Elmer) scanning auger microprobe (SAM), fitted with a LaB_6 electron gun. The spectra were acquired at beam currents ranging from 1 to 3 nA, with a primary acceleration voltage of 3 keV. Low beam currents were chosen in order to prevent charging of the analyzed samples. Sputter cleaning was achieved with a 2 keV Ar^+ ion gun in the raster mode, with a sputter rate of about 4 nm/s with respect to Ta_2O_5 . The spectra were acquired in survey mode for identification of the elements and in multiplex mode for quantitative measurements. The base pressure during analysis was about 1×10^{-9} Torr. The concentrations of a given element X was evaluated, on sputter-cleaned samples, using the relationship:

$$C_x = \frac{(I_x/S_x)}{\sum(I_\alpha/S_\alpha)}$$

where I_x and S_x are respectively the peak-to-peak amplitude and the AES sensitivity factors of the element. The summation is over one peak per element present in the specimen. The sensitivity factors at 3 keV used in this work were the following: $S_{\text{Rh}} = 0.640$, $S_{\text{C}} = 0.180$, $S_{\text{Cl}} = 1.100$, $S_{\text{P}} = 0.530$, $S_{\text{O}} = 0.500$, $S_{\text{N}} = 0.350$; $S_{\text{F}} = 0.480$. Surface mapping and depth profiling were carried out to study the distribution of the elements at the surface and in the bulk of the deposits, respectively.

3. Results

Fig. 1 shows the AES spectra of sample no. 1 (dotted line) and of a Rh standard (full line), acquired after Ar^+ sputter cleaning. The presence of Rh in the deposit is revealed by the characteristic peaks of the element (MNN triplet at 225, 256 and 302 eV and LMM singlet at 46 eV). The other peaks present in the spectrum of the deposit reveal the presence of P (LMM singlet at 120 eV), Cl (KLL singlet 180 eV), N (KLL singlet at 375 eV) and O (KLL singlet at 510 eV). No

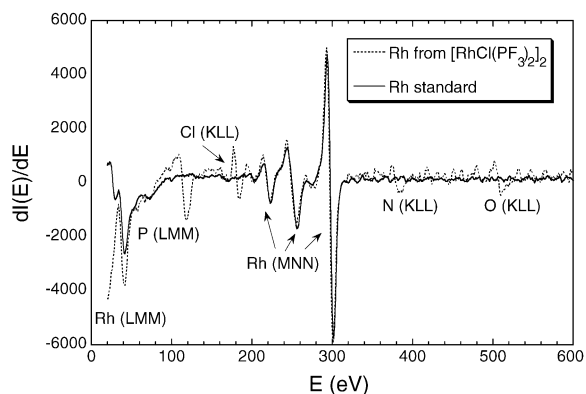


Fig. 1. Auger survey spectrum of a deposit grown from $[\text{RhCl}(\text{PF}_3)_2]_2$ (sample no. 1, gray line) compared with the spectrum of a pure Rh standard (full line). The characteristic peaks are at 46, 225, 256, and 302 eV for Rh, 180 eV for Cl, 120 eV for P, 380 eV for N and 510 eV for O.

F is detected even though this element is present at high concentrations in the precursor molecule. The AES spectrum therefore indicates that the deposit contains impurities due both to partial precursor decomposition (P and Cl) and to air uptake (N and O). The presence of C cannot be completely excluded, since the C KLL peak is located in the same region as the Rh triplet, between 260 and 270 eV. Spectra with similar features were recorded on more than 10 samples, grown from $[\text{RhCl}(\text{PF}_3)_2]_2$ under different experimental conditions. No significant differences in the relative intensity of the peaks were detected between spectra acquired in area mode or point mode.

After identification of the elements, we performed AES mapping in order to study their spatial distribution across the deposit surface. Fig. 2 shows surface AES chemical maps of the elements Rh, Cl, O and P. These maps were acquired over a selected energy region, containing the peak of interest. The probing electron beam was scanned in the rectangular frame in Fig. 2 and at each point an Auger spectrum was taken. After extraction of the elemental peak intensities, the maps in Fig. 2 were obtained. The elements Rh, Cl, O and P are homogeneously distributed across the deposit surface, with the exception of the area marked by the circle in the maps of Rh, O and P and of the right side region of the Rh map. Here the Rh concentration is higher than in the rest of the deposit. The N map (not reported) also

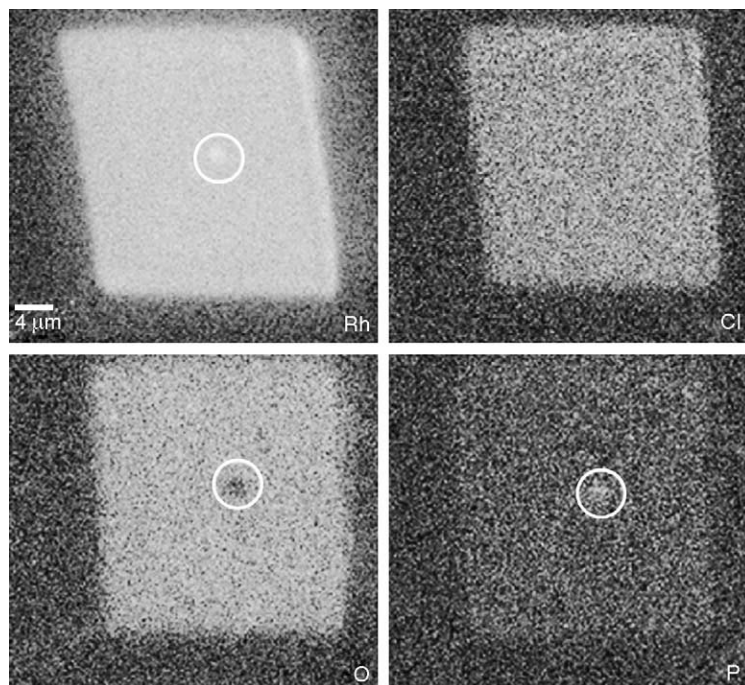


Fig. 2. Scanning auger maps of the elements Rh, Cl, O, P acquired on sample no. 1.

reveals a homogeneous distribution of the element. This result shows that the surface chemical composition of the deposits is homogeneous within the AES lateral resolution limit. Nevertheless this does not exclude inhomogeneities at a smaller scale, as previously observed by TEM/EELS analysis [17].

Before evaluating the elemental concentrations we performed a comparative AES analysis to exclude the presence of C in the deposit. Actually, even if C is absent in the precursor it may be present in EBID structures due to contamination of the deposition system. Fig. 3 shows the AES spectra of a deposit grown by EBID of $[\text{RhCl}(\text{PF}_3)_2]_2$ compared to a C standard, in the interval 220–340 eV. Since different types of C (carbide, amorphous, adventitious etc.) give very different AES curve shapes, here we used as C standard a square grown by EBID from the precursor $(\text{CH}_3)_2\text{Au}(\text{tfa})$, containing about 70 at.% C. The plot shows that the C characteristic C (KLL) singlet at 265 eV is absent in the spectrum of the Rh containing sample. This applies to all deposits grown from $[\text{RhCl}(\text{PF}_3)_2]_2$ studied here, therefore they are considered carbon-free within the detection limit of our AES analysis. This detection limit, being

determined both by the AES sensitivity limit for C (about 0.5 at.%) and by the peak-to-peak amplitude of the noise signal of the spectra, can be reasonably considered around 2 at.%.

The chemical composition of 12 samples, grown with varying electron current (I_p), exposure time (t_e)

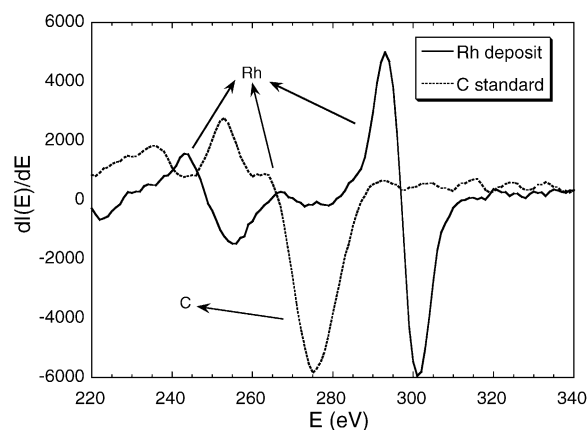


Fig. 3. Comparison of AES spectra of deposits grown from $[\text{RhCl}(\text{PF}_3)_2]_2$ (solid line, sample no. 1) and $(\text{CH}_3)_2\text{Au}(\text{tfa})$ (dotted line, sample no. 2) in the energy range between 220 and 340 eV.

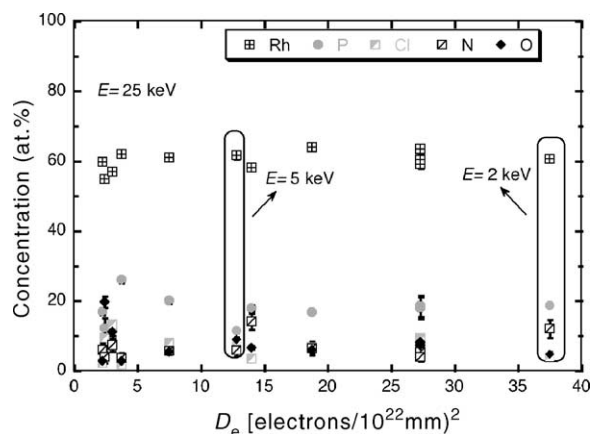


Fig. 4. Atomic concentrations vs. electron dose of the elements Rh, P, Cl, N and O determined by AES. The concentration values refer to deposit grown with $E = 25$ keV, unless otherwise indicated in the figure. The error bars were evaluated by measuring the peak-to-peak amplitude of the noise signal. The error bars for the Rh concentrations are smaller than the symbols.

and irradiated surface (A) are reported in Fig. 4 versus the electron dose $D_e = I_p t_e / A n_f$, where n_f is the number of scanned frames per second. Three different values of the electron energy (E) where used for deposition: 25 keV (value at which most of the deposits where carried out), 5 and 2 keV (values contained in areas delimited by the rounded rectangles). The plot shows no systematic composition change on varying the electron dose between 3×10^{22} and 4×10^{23} electrons/ μm^2 . In addition no significant effects on the chemical composition were detected depositing at the three different employed electron energies. The large scatter of the values depends upon the reproducibility of both the analytical technique and the deposition process. Sources of systematic errors in the AES of EBID structures can arise from differences in morphology of the analyzed samples, matrix effects, nanocomposite structure of the samples, effect of preferential sputtering. Interestingly, the peak-to-peak intensity of the various elements remains stable during prolonged multiplex acquisition, indicating that no significant ex situ electron beam induced chemical changes of the deposited material occur during AES. The chemical composition, averaged over twelve deposits was found to be: 60.1 ± 0.6 at.% Rh, 18.7 ± 2.0 at.% P, 6.8 ± 0.8 at.% Cl, 7.5 ± 1.0 at.% O and 6.6 ± 1.6 at.% N.

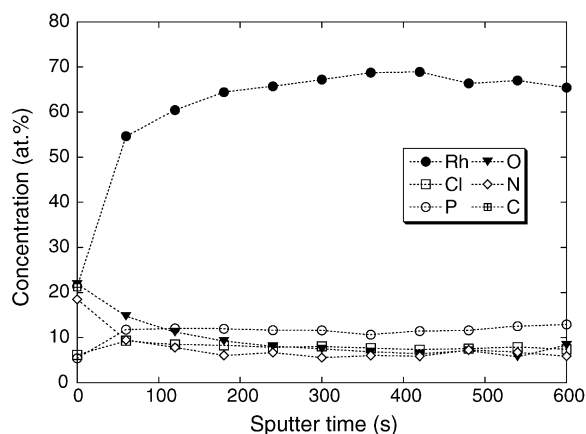


Fig. 5. Auger depth profile of sample no. 3. The plot reports the concentration of the elements versus the sputter time. The sputter rate is about 4 nm/s with respect to Ta_2O_5 .

To gain more insight into the chemical composition of the deposit bulk, we performed AES depth profiling. The AES depth profile spectrum of sample no. 3 is shown in Fig. 5. A contamination layer containing the elements C, N and O covers the as-received sample (sputter time = 0 s). By progressive removal of the contamination layer, the concentrations of C, N and O sharply decrease whereas the P, Cl and Rh concentrations increase. After complete removal of the contamination layer the concentrations of the elements reach a stable value and show no significant changes with increasing deposit depth.

For a comparative study, EBID of Rh was also performed using the commercial precursor $[\text{RhCl}(\text{CO})_2]_2$. The spectrum of sample no. 4 is shown in Fig. 6. It reveals the presence of Rh, Cl (see above for the localization of the characteristic peaks) and C (KLL singlet peak is clearly visible at 275 eV, within the Rh triplet). The N and O peaks, close to the background noise level, are visible only in multiplex mode. The chemical composition, averaged over two deposits, under the same experimental conditions ($E = 25$ keV, $I_p = 2.2$ nA), was found to be: 56.5 ± 1.7 at.% Rh, 33.8 ± 3.5 at.% C, 4.8 ± 0.8 at.% Cl, 3.0 ± 1.5 at.% N, and 2.0 ± 1.5 at.% O.

The Rh and Cl concentrations in deposits obtained from the two Rh precursors are similar. The elements bonded directly to Rh atoms, P and C, are found in high concentrations in the two different deposits. In both cases the most electro-negative elements present

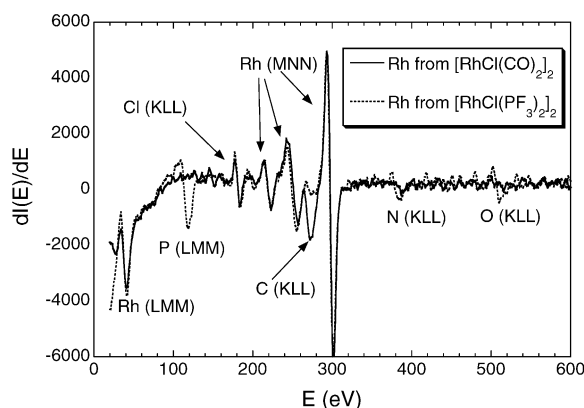


Fig. 6. Comparison of AES spectra of deposits grown from $[\text{RhCl}(\text{PF}_3)_2]_2$ (full line) and $[\text{RhCl}(\text{CO})_2]_2$ (dotted line) under the same experimental conditions (samples no. 1 and 4).

in the molecules (F and O) are absent. Nitrogen is found in both cases but the concentrations in the deposits obtained from $[\text{RhCl}(\text{PF}_3)_2]_2$ are slightly higher. Interestingly, the deposits grown from $[\text{RhCl}(\text{CO})_2]_2$ contain less O, despite the presence of the element in the precursor.

4. Discussion

EBID performed from $[\text{RhCl}(\text{PF}_3)_2]_2$ gives a solid containing 60.1 ± 0.6 at.% Rh, 18.7 ± 2 at.% P, 6.8 ± 0.8 at.% Cl, 7.5 ± 1 at.% O and 6.6 ± 1.6 at.% N. The presence of Rh, Cl and P is explained by partial decomposition of the precursor molecule. It is not clear whether the presence of O and N can be explained by co-deposition or air uptake after exposure to the atmosphere. The N and O concentrations remain unchanged even after several days of pumping in a vacuum of 10^{-9} Torr, revealing that the elements are part of a stable solid compound. The presence of P, in almost the same amount as in the precursor, and the absence of F in the deposits indicates that the PF_3 ligands are decomposed under electron irradiation and are not released as trifluorophosphine (PF_3), as described in the proposed mechanism for thermal CVD of Rh from the same precursor [11]. Chlorine is also found in some cases in thermal CVD deposits obtained from the same precursor [22].

EBID using $[\text{RhCl}(\text{CO})_2]_2$ gives a solid containing 56.5 ± 1.7 at.% Rh, 33.8 ± 3.5 at.% C, $4.8 \pm$

0.8 at.% Cl, 3.0 ± 1.5 at.% N, and 2.0 ± 1.5 at.% O. In this case the contamination seems to be caused mainly by partial decomposition of the precursor. The presence of C and the low O content indicate a dissociation of the CO ligands under electron irradiation (as in the case of PF_3).

The chemical composition of deposits grown from the two different precursors confirms that the processes involved in EBID are different from low-pressure thermal chemical vapor deposition processes. Mass spectrometry already reveals the difference from thermal decomposition by the high amount of P^+ obtained under electron ionization, as discussed in the comparison with the density functional theory (DFT) calculations [16]. EBID is therefore more likely the result of a complex reaction path, which includes multiple ionization and re-arrangements of products of primary decomposition reactions. In any case, strong similarities were observed in the chemical composition of deposits grown from the two precursors, which suggests a similar decomposition mechanism. In both cases the most electronegative elements, constituting the outer shell of the molecules, are absent in the solids whereas the elements constituting the core of the molecules are present in similar concentrations. This can be tentatively explained by a preferential electron attachment leading to the detachment of F and O outer atoms.

For deposits grown from $[\text{RhCl}(\text{PF}_3)_2]_2$ the chemical composition does not vary with the electron dose. This suggests that a stable solid compound forms at electron doses lower than those investigated in this work and that its composition remains stable under further electron irradiation. The weak effect on the chemical composition of the electron energy between 2 and 25 keV is an indication of the low selectivity of the EBID process for electron energies in the keV range. Nevertheless our results do not exclude that intermediate compounds, with different chemical compositions, form at lower electron doses and electron energies (in the eV range). The stability of the deposit under electron irradiation excludes that significant compositional changes, due to electron beam induced reactions, occur during AES. This is confirmed by the fact that the peak-to-peak intensities of the elements are constant during continuous irradiation (irradiation time of about 30 min, with $I_p = 5$ nA).

5. Conclusion

EBID of rhodium was carried out from the precursors $[\text{RhCl}(\text{PF}_3)_2]_2$ and, for the first time, $[\text{RhCl}(\text{CO})_2]_2$. $[\text{RhCl}(\text{PF}_3)_2]_2$ gives deposits containing about 60 at.% Rh, 19 at.% P, 7 at.% Cl, 7 at.% O and 6 at.% N. The chemical compositions of such deposits are not significantly affected by variations in electron dose or electron energy. Surface mapping and depth profiling reveal that the elements are homogeneously distributed at the deposit surface and in the deposit bulk. $[\text{RhCl}(\text{CO})_2]_2$ gives deposits containing about 56 at.% Rh, 34 at.% C, 5 at.% Cl, and traces N and O. The strong similarities in chemical composition of deposits grown from different precursors indicate a similar decomposition mechanism.

Acknowledgement

This work was partially financed by the Swiss National Science Fund of Research (SNF No. 21-64064.00) and by CTI-TN 5441-2.

References

- [1] C. Schossler, J. Urban, H.W.P. Koops, *J. Vac. Sci. Technol. B* 15 (1997) 1535.
- [2] H.W.P. Koops, *Proc. SPIE* 2849 (1996) 248.
- [3] M. Weber, M. Rudolph, J. Kretz, H.W.P. Koops, *J. Vac. Sci. Technol. B* 13 (1995) 279.
- [4] H.W.P. Koops, C. Schlosser, A. Kaya, M. Weber, *J. Vac. Sci. Technol. B* 14 (1996) 4105.
- [5] P.C. Hoyle, J.R.A. Cleaver, H. Ahmed, *J. Vac. Sci. Technol. B* 14 (1996) 662.
- [6] I. Utke, B. Dwir, K. Leifer, F. Cicoira, P. Doppelt, P. Hoffmann, E. Kapon, *Microelectron. Eng.* 53 (2000) 261.
- [7] I. Utke, P. Hoffmann, B. Dwir, K. Leifer, E. Kapon, P. Doppelt, Focused electron beam induced deposition of gold, *J. Vac. Sci. Technol. B* 18 (2000) 3168.
- [8] I. Utke, R. Berger, L. Scandella, P. Hoffmann, *Appl. Phys. Lett.* 80 (2002) 4792.
- [9] O. Sqalli, I. Utke, P. Hoffmann, F. Marquis-Weible, *J. Appl. Phys.* 92 (2002) 1078.
- [10] S. Matsui, K. Mori, *J. Vac. Sci. Technol. B* 4 (1985) 299.
- [11] P. Doppelt, L. Ricard, V. Weigel, *Inorg. Chem.* 32 (1993) 1039.
- [12] F. Marchi, D. Tonneau, H. Dallaporta, V. Safarof, V. Bouchiat, P. Doppelt, R. Even, L. Beitone, *J. Vac. Sci. Technol. B* 18 (2000) 1171.
- [13] P. Hoffmann, I. Utke, F. Cicoira, B. Dwir, K. Leifer, E. Kapon, P. Doppelt, *MRS Symp. Proc.* 624 (2000) 171.
- [14] P. Hoffmann, I. Utke, F. Cicoira, *SPIE Proc.* 5023 (2003) 4.
- [15] T. Ohta, F. Cicoira, P. Doppelt, L. Beitone, P. Hoffmann, *Chem. Vap. Depos.* 7 (2001) 33.
- [16] P. Seuret, F. Cicoira, T. Ohta, P. Doppelt, P. Hoffmann, J. Weber, T. Wesolowski, *Phys. Chem. Chem. Phys.* 5 (2003) 268.
- [17] F. Cicoira, K. Leifer, P. Hoffmann, I. Utke, B. Dwir, D. Laub, P.A. Buffat, E. Kapon, P. Doppelt, *J. Cryst. Growth* 265 (2004) 619.
- [18] NIST Mass Spectrometry Data Center, <http://webbook.nist.gov/chemistry>.
- [19] J.C. Hierso, P. Serp, R. Feurer, P. Kalk, *Appl. Organomet. Chem.* 12 (1998) 161.
- [20] M.A. Bennet, J. Patmore, *Inorg. Chem.* 10 (1971) 2387.
- [21] A. Luisier, I. Utke, T. Bret, F. Cicoira, R. Hauert, S.-W. Rhee, P. Doppelt, P. Hoffmann, *J. Electrochem. Soc.*, (2004) in press.
- [22] P. Doppelt, V. Weigel, P. Guinot, *Mater. Sci. Engineer. B* 17 (1993) 143.